

# Spin effects in Kapitza-Dirac scattering at light with elliptical polarization

Rico Erhard and Heiko Bauke\*

Max-Planck-Institut für Kernphysik, Saupfercheckweg 1, 69117 Heidelberg, Germany

The Kapitza-Dirac effect, which refers to electron scattering at standing light waves, is studied in the Bragg regime with counterpropagating elliptically polarized electromagnetic waves with the same intensity, wavelength, and degree of polarization for two different setups. In the first setup, where the electric field components of the counterpropagating waves have the same sense of rotation, we find distinct spin effects. The spins of the scattered electrons and of the nonscattered electrons, respectively, precess with a frequency that is of the order of the Bragg-reflection Rabi frequency. When the electric-field components of the counterpropagating waves have an opposite sense of rotation, which is the second considered setup, the standing wave has linear polarization, and no spin effects can be observed. Our results are based on numerical solutions of the time-dependent Dirac equation and the analytical solution of a relativistic Pauli equation, which accounts for the leading relativistic effects.

PACS numbers: 03.65.Pm, 31.15.aj

## 1. Introduction

Kapitza-Dirac scattering [1, 2], which is the scattering of massive particles on a standing light wave, emerges as a remarkable consequence of the wave-particle duality of quantum objects. When Kapitza and Dirac first predicted electron scattering at a standing light wave in 1933, an experimental realization was out of reach. The advent of high-intensity laser facilities, however, rendered such an experimental realization possible. The first clear observations of the Kapitza-Dirac effect in the so-called Bragg regime were achieved by employing atoms [3, 4] in 1986 [5] and in the so-called diffraction regime [6] in 1988. Recently, strong-field Kapitza-Dirac scattering of neutral atoms was realized through frustrated tunneling ionization leading to an extreme acceleration of the employed helium atoms [7]. The Kapitza-Dirac effect with electrons was first achieved in 1988 [8] in the diffraction regime. The scattering of electrons in the Bragg regime was demonstrated experimentally in 2001 [9, 10], which comes closest to the diffraction process as proposed originally by Kapitza and Dirac [1]. These experiments stimulated also renewed theoretical interest in this effect [11–13] and generalizations thereof. For example, in Refs. [14, 15] two-particle Kapitza-Dirac scattering was studied, and also Kapitza-Dirac scattering of electrons from a bichromatic standing light wave with linear polarization [16] or circular polarization [17] has been considered recently. In dielectric media, electrons may also diffract from traveling light waves [18].

As the electron couples to electromagnetic fields not only via its charge but also via its spin degree of freedom, it is natural to ask if electron-spin dynamics may be observed in the Kapitza-Dirac effect [9]. Freimund and Batelaan found a vanishingly small spin-flip probability in the investigated laser setup and parameter regime by simulating the Bargmann-Michel-Telegdi equations [19]. Another derivation [20] solved the Pauli equation perturbatively via second-quantization methods in the diffraction regime but only found tiny spin effects for a setup with linearly polarized light waves. Spin effects,

however, can be observed in the Kapitza-Dirac effect if the electron enters the laser field with a certain relativistic initial momentum, which must fulfill a spin-flip resonance condition [21, 22], or in specific laser setups with circular polarization [17].

As a result of emerging novel high-intensity light sources such as the Extreme Light Infrastructure Ultra High Field Facility, which envisage to provide field intensities in excess of  $10^{20}$  W/cm<sup>2</sup> and field frequencies in the x-ray domain [23], spin effects in relativistic light-matter interaction became of wide interest [24–28]. In particular, the interaction between the electron's spin and the degree of elliptical polarization of an external strong electromagnetic field has been considered. For example, it was recently shown that electrons scattering non-resonantly at standing light waves of counterpropagating plane waves with elliptical polarization can exhibit spin precession [29, 30]. Strong spin effects have also been found in electron-positron pair production in strong electromagnetic fields with elliptical polarization [31, 32] as well as in strong-field ionization via electromagnetic fields with elliptical polarization [33, 34].

In this paper we will study the Kapitza-Dirac effect with electrons in standing light waves of counterpropagating plane waves with elliptical polarization and especially study possible spin effects. This article is organized as follows: In Sec. 2 we will specify the considered configurations of the time-dependent electromagnetic fields. The effect of the fast oscillating fields can be described by time-independent ponderomotive potentials, which will be derived in Sec. 3. The resulting time evolution by the ponderomotive potentials will be determined analytically and compared to a numerical solution of the time-dependent Dirac equation in Sec. 4. A summary and our conclusions follow in Sec. 5.

---

\* heiko.bauke@mpi-hd.mpg.de

## 2. Electrons in counterpropagating electromagnetic waves with elliptical polarization

Electron scattering at a standing light wave, which is composed of two counterpropagating laser waves with equal wavelength  $\lambda$ , equal electric field amplitude  $\hat{E}$ , and the same degree of ellipticity, will be considered. Depending on the relative sense of rotation of the electric-field component of the two plane-wave fields traveling along the  $x$  axis, the electric- and magnetic-field components are given by

$$\mathbf{E}_{1,2}^{\zeta\zeta}(x,t) = \hat{E} \begin{pmatrix} 0 \\ \cos(kx \mp \omega t) \\ \cos(kx \mp \omega t \pm \eta) \end{pmatrix}, \quad (1a)$$

$$\mathbf{B}_{1,2}^{\zeta\zeta}(x,t) = \frac{\hat{E}}{c} \begin{pmatrix} 0 \\ \mp \cos(kx \mp \omega t \pm \eta) \\ \pm \cos(kx \mp \omega t) \end{pmatrix}, \quad (1b)$$

or

$$\mathbf{E}_{1,2}^{\zeta\zeta}(x,t) = \hat{E} \begin{pmatrix} 0 \\ \cos(kx \mp \omega t) \\ \cos(kx \mp \omega t + \eta) \end{pmatrix}, \quad (2a)$$

$$\mathbf{B}_{1,2}^{\zeta\zeta}(x,t) = \frac{\hat{E}}{c} \begin{pmatrix} 0 \\ \mp \cos(kx \mp \omega t + \eta) \\ \pm \cos(kx \mp \omega t) \end{pmatrix}, \quad (2b)$$

respectively, where  $c$  denotes the speed of light,  $k = 2\pi/\lambda$  is the wave number, and  $\omega = 2\pi c/\lambda$ . The parameter  $\eta \in (-\pi, \pi]$  determines the degree of ellipticity, with  $\eta = 0$  and  $\eta = \pi$  corresponding to linear polarization and  $\eta = \pm\pi/2$  corresponding to circular polarization. The two electromagnetic waves given by (1a) and (1b) rotate in parallel (corotating setup), whereas the two electromagnetic waves given by (2a) and (2b) rotate opposite to each other (antirotating setup); see Fig. 1 for an illustration. The total electromagnetic fields and the corresponding vector potentials of these setups follow as

$$\mathbf{E}^{\zeta\zeta}(x,t) = 2\hat{E} \cos(kx) \begin{pmatrix} 0 \\ \cos(\omega t) \\ \cos(\omega t - \eta) \end{pmatrix}, \quad (3a)$$

$$\mathbf{B}^{\zeta\zeta}(x,t) = \frac{2\hat{E}}{c} \sin(kx) \begin{pmatrix} 0 \\ -\sin(\omega t - \eta) \\ \sin(\omega t) \end{pmatrix}, \quad (3b)$$

$$\mathbf{A}^{\zeta\zeta}(x,t) = -\frac{2\hat{E}}{\omega} \cos(kx) \begin{pmatrix} 0 \\ \sin(\omega t) \\ \sin(\omega t - \eta) \end{pmatrix} \quad (3c)$$

for the corotating setup and

$$\mathbf{E}^{\zeta\zeta}(x,t) = 2\hat{E} \cos(\omega t) \begin{pmatrix} 0 \\ \cos(kx) \\ \cos(kx + \eta) \end{pmatrix}, \quad (4a)$$

$$\mathbf{B}^{\zeta\zeta}(x,t) = \frac{2\hat{E}}{c} \sin(\omega t) \begin{pmatrix} 0 \\ -\sin(kx + \eta) \\ \sin(kx) \end{pmatrix}, \quad (4b)$$

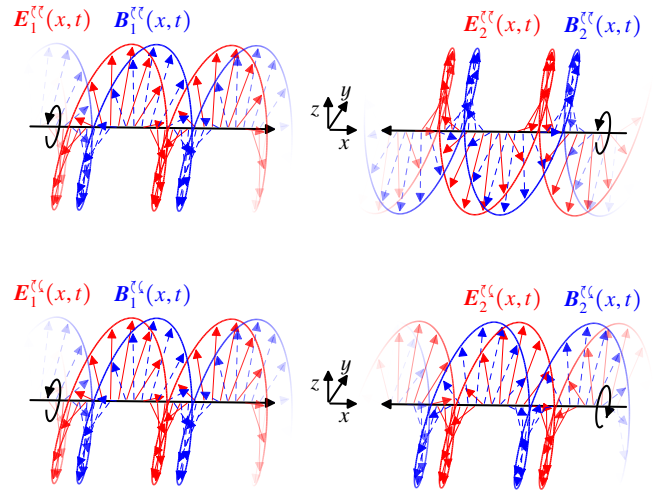


**FIG. 1:** (Color online) Schematic illustration of the two considered field configurations. Two electromagnetic plane waves with elliptical polarization traveling into opposite directions are superimposed. The sense of rotation of the electric field vector may be (top) equal (corotating setup) or (bottom) opposite (antirotating setup). The sense of rotation and the propagation direction are indicated by black arrows, red solid arrows represent electric-field components, and blue dashed arrows represent magnetic-field components.

$$\mathbf{A}^{\zeta\zeta}(x,t) = -\frac{2\hat{E}}{\omega} \sin(\omega t) \begin{pmatrix} 0 \\ \cos(kx) \\ \cos(kx + \eta) \end{pmatrix} \quad (4c)$$

for the antirotating setup, respectively.

The quantum-mechanical evolution of an electron of mass  $m$  and charge  $q = -e$  in the laser field with the vector potential (3c) or (4c) is governed by the quasi-one-dimensional Dirac equation

$$i\hbar\psi(x,t) = \left( -c\hat{n}\alpha_x \frac{\partial}{\partial x} - cq\omega(t)\alpha \cdot \mathbf{A}(x,t) + mc^2\beta \right) \Psi(x,t) \quad (5)$$

with the Dirac matrices  $\alpha = (\alpha_x, \alpha_y, \alpha_z)^\top$  and  $\beta$  [35, 36] and the reduced Planck constant  $\hbar$ . This form of the Dirac equation can be justified by starting from the fully three-dimensional Dirac equation and noting that the canonical momentum is preserved in the  $y$  and in  $z$  directions due to the special form of the vector potentials (3c) and (4c). Thus, the three-dimensional Dirac equation separates into three one-dimensional equations, of which one is given by (5) and the remaining two describe free motion in the  $y$  and in  $z$  directions. In (5) the window function

$$w(t) = \begin{cases} \sin^2 \frac{\pi t}{2\Delta T} & \text{if } 0 \leq t \leq \Delta T, \\ 1 & \text{if } \Delta T \leq t \leq T - \Delta T, \\ \sin^2 \frac{\pi(T-t)}{2\Delta T} & \text{if } T - \Delta T \leq t \leq T \end{cases} \quad (6)$$

has been introduced, which allows for a smooth turn-on and turn-off of the laser field.

In Sec. 4 we will present numerical solutions of the time-dependent Dirac equation (5) which are obtained solving this equation on a one-dimensional grid of size  $\lambda$  with periodic boundary conditions by a Fourier split-operator method [37, 38].

Due to the periodic boundary condition the wave function can be expanded into a discrete set of momentum eigenstates

$$\psi_n^\gamma(x) = \sqrt{\frac{k}{2\pi}} u_n^\gamma e^{inkx}, \quad (7)$$

which are simultaneous eigenstates of the free Dirac Hamiltonian, the  $x$  component of the canonical momentum operator (with eigenvalue  $nk\hbar$ ), and the  $z$  component of the Foldy-Wouthuysen spin operator [39]. The upper index  $\gamma \in \{+\uparrow, -\uparrow, +\downarrow, -\downarrow\}$  in  $\psi_n^\gamma(x)$  indicates the spin state, and the sign of the energy eigenvalue and  $u_n^\gamma$  is defined as

$$u_n^{+\uparrow/+ \downarrow} = \sqrt{\frac{\mathcal{E}_n + mc^2}{2\mathcal{E}_n}} \begin{pmatrix} \chi^{\uparrow/\downarrow} \\ \frac{nk\hbar\sigma_z}{\mathcal{E}_n + mc^2} \chi^{\uparrow/\downarrow} \end{pmatrix}, \quad (8a)$$

$$u_n^{-\uparrow/- \downarrow} = \sqrt{\frac{\mathcal{E}_n + mc^2}{2\mathcal{E}_n}} \begin{pmatrix} -\frac{nk\hbar\sigma_z}{\mathcal{E}_n + mc^2} \chi^{\uparrow/\downarrow} \\ \chi^{\uparrow/\downarrow} \end{pmatrix}, \quad (8b)$$

with  $\chi^\uparrow = (1, 0)^\top$  and  $\chi^\downarrow = (0, 1)^\top$  and the relativistic energy-momentum relation

$$\mathcal{E}_n = \sqrt{(mc^2)^2 + (nk\hbar)^2}. \quad (9)$$

In the so-called Bragg regime of the Kapitza-Dirac effect [2, 13] the electron has to meet the resonance condition, which requires that the electron's momentum in the propagation direction of the light field equals  $\pm\hbar k$ . Thus, we will employ  $\psi_{-1}^{\uparrow/\downarrow}(x)$  as a canonical initial quantum state.

### 3. Ponderomotive potentials

The Bragg regime of the Kapitza-Dirac effect is realized for sufficiently weak electromagnetic fields, more precisely, if the energy that is gained in a single laser cycle, which is of the order  $c|q|\hat{E}/\omega$ , is small compared to the energy of a single photon, which is  $\hbar\omega$ . Furthermore, we will assume that the electron's kinetic energy remains small compared to its rest mass energy  $mc^2$  for all times. Thus,  $c|q|\hat{E}/\omega \ll \hbar\omega < mc^2$ . As a consequence of the Bragg condition, nonrelativistic initial momentum implies  $\lambda \gg \lambda_C = \hbar/(mc)$ , where  $\lambda_C$  is the electron's reduced Compton wavelength. The nonrelativistic electron momentum justifies the application of a weakly relativistic theory. The weakly relativistic limit of the Dirac equation may be reached via a Foldy-Wouthuysen transformation [39, 40], which yields, for a now two-component wave function  $\Psi(\mathbf{r}, t)$ ,

$$\begin{aligned} i\hbar\dot{\Psi}(\mathbf{r}, t) = & \left( \frac{(-i\hbar\nabla - q\mathbf{A}(\mathbf{r}, t))^2}{2m} - \frac{q\hbar}{2m} \boldsymbol{\sigma} \cdot \mathbf{B}(\mathbf{r}, t) \right. \\ & - \frac{(-i\hbar\nabla - q\mathbf{A}(\mathbf{r}, t))^4}{8m^3c^2} - \frac{q^2\hbar^2}{8m^3c^4} (c^2\mathbf{B}(\mathbf{r}, t)^2 - \mathbf{E}(\mathbf{r}, t)^2) \\ & - \frac{q\hbar}{4m^2c^2} \boldsymbol{\sigma} \cdot (\mathbf{E}(\mathbf{r}, t) \times (-i\hbar\nabla - q\mathbf{A}(\mathbf{r}, t))) - \frac{q\hbar^2}{8m^2c^2} \nabla \cdot \mathbf{E}(\mathbf{r}, t) \\ & \left. + \frac{q\hbar}{8m^3c^2} \left\{ \boldsymbol{\sigma} \cdot \mathbf{B}(\mathbf{r}, t), (-i\hbar\nabla - q\mathbf{A}(\mathbf{r}, t))^2 \right\} \right) \Psi(\mathbf{r}, t), \quad (10) \end{aligned}$$

with the magnetic vector potential  $\mathbf{A}(\mathbf{r}, t)$  and  $\mathbf{B}(\mathbf{r}, t) = \nabla \times \mathbf{A}(\mathbf{r}, t)$ ,  $\mathbf{E}(\mathbf{r}, t) = -\dot{\mathbf{A}}(\mathbf{r}, t)$ , and the vector of Pauli matrices  $\boldsymbol{\sigma} = (\sigma_x, \sigma_y, \sigma_z)^\top$ . Taking into account that the electron's kinematic momentum remains small compared to  $mc$  and that  $\lambda \gg \lambda_C = \hbar/(mc)$  allows us to neglect various terms in Eq. (10), and the specific form of the vector potentials (3c) and (4c) leads finally to

$$\begin{aligned} i\hbar\dot{\Psi}(x, t) = & \left( -\frac{\hbar^2}{2m} \frac{\partial^2}{\partial x^2} + \frac{q^2}{2m} \mathbf{A}(x, t)^2 - \frac{q\hbar}{2m} \boldsymbol{\sigma} \cdot \mathbf{B}(x, t) \right. \\ & \left. - \frac{q\hbar}{4m^2c^2} \boldsymbol{\sigma} \cdot (\mathbf{E}(x, t) \times (-i\hbar\nabla_x - q\mathbf{A}(x, t))) \right) \Psi(x, t), \quad (11) \end{aligned}$$

where  $\nabla_x$  denotes the differential operator  $\nabla_x = (\partial_x, 0, 0)^\top$ . This is the nonrelativistic Pauli equation, which is amended by a relativistic correction due to spin-orbit coupling ( $\sim \mathbf{E} \times (-i\hbar\nabla_x)$ ) and the coupling of the electron's spin to the photonic spin density of the electromagnetic wave ( $\sim \mathbf{E} \times \mathbf{A}$ ) [29, 30]. It incorporates the dominating terms of (10) that account for the electron's spatial motion as well as for the spin dynamics.

As shown in [13] for the case of linear polarization, the Kapitza-Dirac effect can be modeled by a time-independent Hamiltonian with suitable ponderomotive potentials. Thus, it appears attractive to replace the time-dependent Hamiltonian in Eq. (11) by a time-independent Hamiltonian, which we will derive in the following by means of a Magnus expansion [41, 42]. The Magnus expansion gives an exponential representation of the solution of a first-order homogeneous linear equation of the type

$$\dot{f}(t) = \tilde{H}(t)f(t) \quad (12)$$

in the form

$$f(t) = \exp(\tilde{U}_1(t) + \tilde{U}_2(t) + \dots)f(0). \quad (13)$$

The main advantage of the Magnus expansion is that each truncated series (13) of any order preserves the unitary character of the quantum-mechanical time evolution. Explicitly, the first two terms of the series (13) are

$$\tilde{U}_1(t) = \int_0^t \tilde{H}(t_1) dt_1 \quad (14)$$

and

$$\tilde{U}_2(t) = \frac{1}{2} \int_0^t \int_0^{t_1} [\tilde{H}(t_1), \tilde{H}(t_2)] dt_2 dt_1. \quad (15)$$

The term  $\tilde{U}_2(t)$  and higher-order corrections account for the fact that  $\tilde{H}(t)$  may not commute with itself at different times  $t$  and in this way implement time ordering.

Applying the Magnus expansion in second order to (11) with the vector potential of the corotating case (3c) and the corresponding electromagnetic fields yields

$$\Psi(x, t) = \exp \left( -\frac{it}{\hbar} \left( -\frac{\hbar^2}{2m} \frac{\partial^2}{\partial x^2} + \frac{2q^2 \hat{E}^2}{m\omega^2} \cos^2(kx) - \frac{\hbar q^2 \hat{E}^2}{m^2 c^2 \omega} \sin \eta (\sin^2(kx) - \cos^2(kx)) \sigma_x + \dots \right) \right) \Psi(x, 0), \quad (16)$$

where we have neglected in the exponent terms which do not grow linearly with time and/or are small (compared to the included terms) in the Bragg regime, i. e.,  $|q|\hat{E}/(\omega mc) \ll 1$  with  $\lambda \gg \lambda_C = \hbar/(mc)$ . Equation (16) represents the time-evolution operator of the equation

$$i\hbar \dot{\Psi}(x, t) = \left( -\frac{\hbar^2}{2m} \frac{\partial^2}{\partial x^2} + \frac{2q^2 \hat{E}^2}{m\omega^2} \cos^2(kx) - \frac{\hbar q^2 \hat{E}^2}{m^2 c^2 \omega} \sin \eta (\sin^2(kx) - \cos^2(kx)) \sigma_x \right) \Psi(x, t), \quad (17)$$

which is the searched-for evolution equation with a time-independent Hamiltonian. It equals the Hamiltonian for the case of linear polarization [13] plus a term which accounts for the spin dynamics due to the ellipticity of the electromagnetic field. Thus, we found polarization-dependent ponderomotive forces similar to the situation in Refs. [43, 44]. Note that the spin term originates in equal magnitude from both the Zeeman term  $\sim \mathbf{B} \cdot \boldsymbol{\sigma}$  and the relativistic correction  $\sim (\mathbf{E} \times \mathbf{A}) \cdot \boldsymbol{\sigma}$  (see also [29, 30]).

Similarly, we can apply the Magnus expansion to (11) with the vector potential of the antirotating case (4c) and the corresponding electromagnetic fields, which yields now

$$\Psi(x, t) = \exp \left( -\frac{it}{\hbar} \left( -\frac{\hbar^2}{2m} \frac{\partial^2}{\partial x^2} + \frac{q^2 \hat{E}^2}{m\omega^2} (2 \cos^2(kx + \eta) \cos \eta + 1 - \cos \eta) + \dots \right) \right) \Psi(x, 0), \quad (18)$$

where we have again neglected in the exponent terms which do not grow linearly with time and/or are small in the Bragg regime. Equation (18) represents the time-evolution operator of the equation

$$i\hbar \dot{\Psi}(x, t) = \left( -\frac{\hbar^2}{2m} \frac{\partial^2}{\partial x^2} + \frac{q^2 \hat{E}^2}{m\omega^2} (2 \cos^2(kx + \eta/2) \cos \eta + 1 - \cos \eta) \right) \Psi(x, t). \quad (19)$$

This can be further simplified by a gauge transform, which removes the additive constant, and a suitable shift of the coordinate system to

$$i\hbar \dot{\Psi}(x, t) = \left( -\frac{\hbar^2}{2m} \frac{\partial^2}{\partial x^2} + \frac{2q^2 \hat{E}^2}{m\omega^2} \cos^2(kx) \cos \eta \right) \Psi(x, t). \quad (20)$$

In contrast to (17), the Hamiltonian in (20) involves no spin-coupling terms, which is a consequence of  $\mathbf{E} \times \mathbf{A} = 0$  and the fact that the Zeeman interaction is zero on average (as it commutes with itself at different times) in the antirotating case.

## 4. Analytical solution of the relativistic Pauli equation and numerical results

In the following, we will derive approximate analytical solutions of the relativistic Pauli equations (17) and (20). For this purpose the wave function  $\Psi(x, t)$  is expanded into plane waves as

$$\Psi(x, t) = \sqrt{\frac{k}{2\pi}} \sum_{\substack{n=\dots,-1,0,1,\dots \\ \gamma \in \{\uparrow, \downarrow\}}} c_n^\gamma(t) \chi^\gamma e^{inkx}, \quad (21)$$

with the time-dependent coefficients  $c_n^\uparrow(t)$  and  $c_n^\downarrow(t)$ , which will be conveniently combined into the pair

$$c_n(t) = (c_n^\uparrow(t), c_n^\downarrow(t))^T. \quad (22)$$

The basis functions that are employed in (21) represent states with a well-defined momentum and spin orientation. They form a system of orthonormal functions on  $x \in [0, \lambda]$ . Thus, the evolution equation for  $c_n^\gamma(t)$ , the relativistic Pauli equation in momentum space, can be derived by plugging the ansatz (21) into (17) or (20) and taking the scalar product with  $\sqrt{k/(2\pi)} \chi^{\gamma'} e^{in'kx}$ . We will ignore possible turn-on and turn-off phases in the following, i. e.,  $\Delta T = 0$ , if not otherwise identified.

### 4.1. Corotating fields

Using the expansion (21), the relativistic Pauli equation for corotating fields (17) is given in momentum space by

$$i\hbar \dot{c}_n(t) = \frac{n^2 k^2 \hbar^2}{2m} c_n(t) + \frac{q^2 \hat{E}^2}{2k^2 m c^2} (c_{n-2}(t) + 2c_n(t) + c_{n+2}(t)) + \frac{\hbar q^2 \hat{E}^2 \sin \eta}{2km^2 c^3} \sigma_x (c_{n-2}(t) + c_{n+2}(t)). \quad (23)$$

Odd and even modes are decoupled in Eq. (23). Furthermore, the relation

$$\frac{k^2 \hbar^2}{2m} \gg \frac{q^2 \hat{E}^2}{2k^2 m c^2} > \frac{\hbar q^2 \hat{E}^2 \sin \eta}{2km^2 c^3} \quad (24)$$

holds for the coefficients in Eq. (23) because of the Bragg-regime condition  $c|q|\hat{E}/\omega \ll \hbar\omega < mc^2$ . Thus, it is justified to truncate the equation system, which yields for the odd modes

$$i \begin{pmatrix} \dot{c}_{-3}^\dagger(t) \\ \dot{c}_{-3}^\downarrow(t) \\ \dot{c}_{-1}^\dagger(t) \\ \dot{c}_{-1}^\downarrow(t) \\ \dot{c}_1^\dagger(t) \\ \dot{c}_1^\downarrow(t) \\ \dot{c}_3^\dagger(t) \\ \dot{c}_3^\downarrow(t) \end{pmatrix} = \begin{pmatrix} 9\Omega_1 & 0 & \Omega_2 & \Omega_3' & 0 & 0 & 0 & 0 \\ 0 & 9\Omega_1 & \Omega_3' & \Omega_2 & 0 & 0 & 0 & 0 \\ \Omega_2 & \Omega_3' & \Omega_1 & 0 & \Omega_2 & \Omega_3' & 0 & 0 \\ \Omega_3' & \Omega_2 & 0 & \Omega_1 & \Omega_3' & \Omega_2 & 0 & 0 \\ 0 & 0 & \Omega_2 & \Omega_3' & \Omega_1 & 0 & \Omega_2 & \Omega_3' \\ 0 & 0 & \Omega_3' & \Omega_2 & 0 & \Omega_1 & \Omega_3' & \Omega_2 \\ 0 & 0 & 0 & 0 & \Omega_2 & \Omega_3' & 9\Omega_1 & 0 \\ 0 & 0 & 0 & 0 & \Omega_3' & \Omega_2 & 0 & 9\Omega_1 \end{pmatrix} \begin{pmatrix} c_{-3}^\dagger(t) \\ c_{-3}^\downarrow(t) \\ c_{-1}^\dagger(t) \\ c_{-1}^\downarrow(t) \\ c_1^\dagger(t) \\ c_1^\downarrow(t) \\ c_3^\dagger(t) \\ c_3^\downarrow(t) \end{pmatrix} \quad (25)$$

by introducing the frequencies

$$\Omega_1 = \frac{k^2 \hbar}{2m}, \quad (26a)$$

$$\Omega_2 = \frac{q^2 \hat{E}^2}{2\hbar k^2 m c^2}, \quad (26b)$$

$$\Omega_3 = \frac{q^2 \hat{E}^2}{2km^2 c^3}, \quad (26c)$$

and  $\Omega_3' = \Omega_3 \sin \eta$ . Note that an additive constant  $2\Omega_2$  has not been included on the diagonal of the coefficient matrix in Eq. (25), which can be justified by a suitable gauge transform. The eigenvalues and eigenvectors of this coefficient matrix can be easily calculated by a computer algebra system giving some rather intricate expressions. In the parameter regime, where (24) is fulfilled, the eigenvectors of the coefficient matrix can be approximated by the column vectors of the constant matrix

$$\begin{pmatrix} v_1 & v_2 & v_3 & v_4 & v_5 & v_6 & v_7 & v_8 \end{pmatrix} = \frac{1}{2} \begin{pmatrix} 0 & 0 & 0 & 0 & 1 & 1 & 1 & 1 \\ 0 & 0 & 0 & 0 & 1 & 1 & 1 & 1 \\ 1 & 1 & 1 & 1 & 0 & 0 & 0 & 0 \\ 1 & -1 & -1 & 1 & 0 & 0 & 0 & 0 \\ 1 & -1 & 1 & -1 & 0 & 0 & 0 & 0 \\ 1 & 1 & -1 & -1 & 0 & 0 & 0 & 0 \\ 0 & 0 & 0 & 0 & 1 & -1 & 1 & -1 \\ 0 & 0 & 0 & 0 & 1 & 1 & -1 & -1 \end{pmatrix}, \quad (27)$$

and the corresponding exact eigenvalues are

$$\begin{aligned} \varepsilon_{1,5} &= 5\Omega_1 + \frac{\Omega_2 + \Omega_3'}{2} \\ &\mp \sqrt{(8\Omega_1 - (\Omega_2 + \Omega_3'))^2/4 + (\Omega_2 + \Omega_3')^2}, \end{aligned} \quad (28a)$$

$$\begin{aligned} \varepsilon_{2,6} &= 5\Omega_1 + \frac{-\Omega_2 + \Omega_3'}{2} \\ &\mp \sqrt{(8\Omega_1 - (-\Omega_2 + \Omega_3'))^2/4 + (-\Omega_2 + \Omega_3')^2}, \end{aligned} \quad (28b)$$

$$\begin{aligned} \varepsilon_{3,7} &= 5\Omega_1 + \frac{\Omega_2 - \Omega_3'}{2} \\ &\mp \sqrt{(8\Omega_1 - (\Omega_2 - \Omega_3'))^2/4 + (\Omega_2 - \Omega_3')^2}, \end{aligned} \quad (28c)$$

$$\begin{aligned} \varepsilon_{4,8} &= 5\Omega_1 + \frac{-\Omega_2 - \Omega_3'}{2} \\ &\mp \sqrt{(8\Omega_1 - (-\Omega_2 - \Omega_3'))^2/4 + (-\Omega_2 - \Omega_3')^2}. \end{aligned} \quad (28d)$$

Choosing  $c_{-1}^\dagger(0) = 1$  and  $c_n^\downarrow(0) = 0$  otherwise as the initial condition and approximating the eigenvectors of the coefficient matrix in Eq. (25) by (27) yields the time-dependent solution to (25),

$$c_{-3}^\dagger(t) = 0, \quad (29a)$$

$$c_{-3}^\downarrow(t) = 0, \quad (29b)$$

$$c_{-1}^\dagger(t) = \frac{1}{4} (e^{-i\varepsilon_1 t} + e^{-i\varepsilon_2 t} + e^{-i\varepsilon_3 t} + e^{-i\varepsilon_4 t}), \quad (29c)$$

$$c_{-1}^\downarrow(t) = \frac{1}{4} (e^{-i\varepsilon_1 t} - e^{-i\varepsilon_2 t} - e^{-i\varepsilon_3 t} + e^{-i\varepsilon_4 t}), \quad (29d)$$

$$c_1^\dagger(t) = \frac{1}{4} (e^{-i\varepsilon_1 t} - e^{-i\varepsilon_2 t} + e^{-i\varepsilon_3 t} - e^{-i\varepsilon_4 t}), \quad (29e)$$

$$c_1^\downarrow(t) = \frac{1}{4} (e^{-i\varepsilon_1 t} + e^{-i\varepsilon_2 t} - e^{-i\varepsilon_3 t} - e^{-i\varepsilon_4 t}), \quad (29f)$$

$$c_3^\dagger(t) = 0, \quad (29g)$$

$$c_3^\downarrow(t) = 0. \quad (29h)$$

Note that although the amplitudes  $c_{\pm 3}^{\uparrow/\downarrow}(t)$  are zero, also including modes  $n = \pm 3$  in the truncated system (25) is crucial to describing the Kapitza-Dirac effect properly for corotating fields. The amplitudes  $c_{\pm 3}^{\uparrow/\downarrow}(t)$  vanish only because the approximation (27) has been applied. Employing the exact eigenvectors instead would yield small nonzero amplitudes.

The evolution of the probability  $|c_{-1}^\dagger(t)|^2$  is with (29)

$$\begin{aligned} |c_{-1}^\dagger(t)|^2 &= \frac{1}{16} \left| e^{-i(\varepsilon_2 + \varepsilon_3 + \varepsilon_4)t} + e^{-i(\varepsilon_1 + \varepsilon_3 + \varepsilon_4)t} \right. \\ &\quad \left. + e^{-i(\varepsilon_1 + \varepsilon_2 + \varepsilon_4)t} + e^{-i(\varepsilon_1 + \varepsilon_2 + \varepsilon_3)t} \right|^2. \end{aligned} \quad (30)$$

Considering the regime (24), the following approximations hold:

$$\varepsilon_2 + \varepsilon_3 + \varepsilon_4 \approx 3\Omega_1 - \Omega_2 - \Omega_3' - \frac{3\Omega_2^2 + 3\Omega_3'^2 - 2\Omega_2\Omega_3'}{8\Omega_1}, \quad (31a)$$

$$\varepsilon_1 + \varepsilon_3 + \varepsilon_4 \approx 3\Omega_1 + \Omega_2 - \Omega_3' - \frac{3\Omega_2^2 + 3\Omega_3'^2 + 2\Omega_2\Omega_3'}{8\Omega_1}, \quad (31b)$$

$$\varepsilon_1 + \varepsilon_2 + \varepsilon_4 \approx 3\Omega_1 - \Omega_2 + \Omega_3' - \frac{3\Omega_2^2 + 3\Omega_3'^2 + 2\Omega_2\Omega_3'}{8\Omega_1}, \quad (31c)$$

$$\varepsilon_1 + \varepsilon_2 + \varepsilon_3 \approx 3\Omega_1 + \Omega_2 + \Omega_3' - \frac{3\Omega_2^2 + 3\Omega_3'^2 - 2\Omega_2\Omega_3'}{8\Omega_1}. \quad (31d)$$

Employing these approximations in Eq. (30), some algebraic transformations yield

$$\begin{aligned} |c_{-1}^\dagger(t)|^2 &\approx \cos^2(\Omega_2 t) \cos^2(\Omega_3' t) \\ &\quad + (\sin^2(\Omega_2 t) - \cos^2(\Omega_3' t)) \sin^2\left(\frac{\Omega_2 \Omega_3' t}{4\Omega_1}\right). \end{aligned} \quad (32a)$$

A similar calculation can be carried out for  $|c_{-1}^\downarrow(t)|^2$ ,  $|c_1^\dagger(t)|^2$ , and  $|c_1^\downarrow(t)|^2$ , which finally results in

$$\begin{aligned} |c_{-1}^\downarrow(t)|^2 &\approx \sin^2(\Omega_2 t) \sin^2(\Omega_3' t) \\ &\quad + (-\sin^2(\Omega_2 t) + \cos^2(\Omega_3' t)) \sin^2\left(\frac{\Omega_2 \Omega_3' t}{4\Omega_1}\right), \end{aligned} \quad (32b)$$

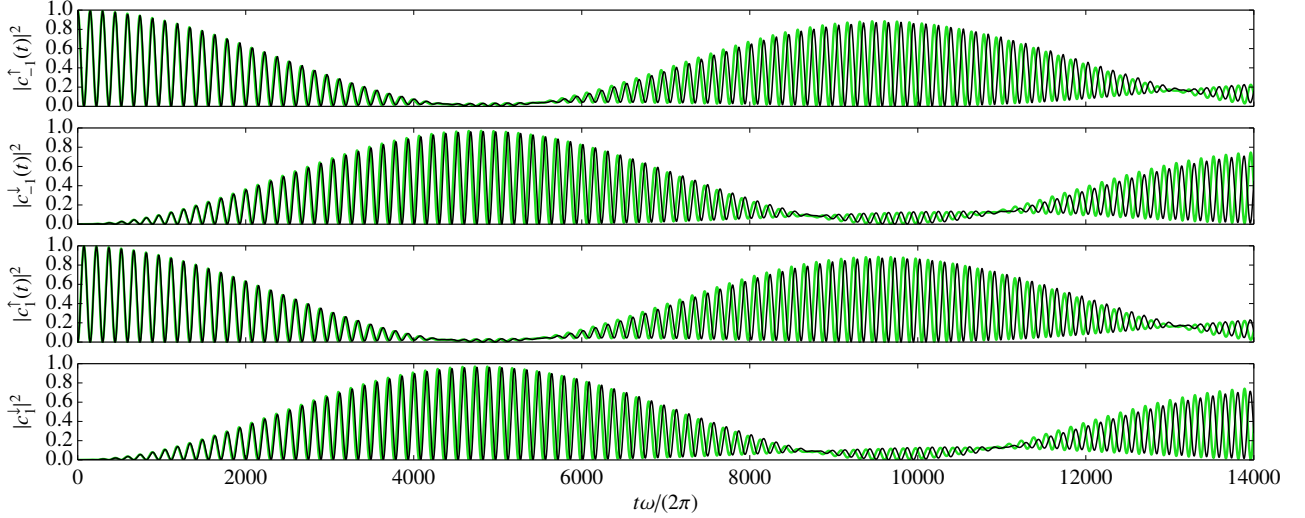


**FIG. 2:** (Color online) Time evolution of the probabilities to find the electron, which interacts with a standing light wave of the corotating setup, in a particular quantum state. Green (gray) lines show, from top to bottom, the analytical results (32a) to (32d) based on the relativistic Pauli equation (17). Black lines represent the corresponding numerical results based on the Dirac equation (5), i. e., the probabilities to find the electron in the states  $\psi_{-1}^{\uparrow}$ ,  $\psi_{-1}^{\downarrow}$ ,  $\psi_1^{\uparrow}$ , and  $\psi_1^{\downarrow}$ , respectively, after the electromagnetic field has been turned off. Parameters are  $\hat{E} = 400$  a.u. =  $2.06 \times 10^{14}$  V/m (corresponding to an intensity of  $1.12 \times 10^{22}$  W/cm<sup>2</sup>),  $\lambda = 3$  a.u. =  $0.159$  nm,  $\Delta T = 10\pi/\omega$ , and  $\eta = \pi/2$ , corresponding to circular polarization.

$$|c_1^{\uparrow}(t)|^2 \approx \sin^2(\Omega_2 t) \cos^2(\Omega_3' t) + (-\sin^2(\Omega_2 t) + \sin^2(\Omega_3' t)) \sin^2\left(\frac{\Omega_2 \Omega_3' t}{4\Omega_1}\right), \quad (32c)$$

$$|c_1^{\downarrow}(t)|^2 \approx \cos^2(\Omega_2 t) \sin^2(\Omega_3' t) + (\sin^2(\Omega_2 t) - \sin^2(\Omega_3' t)) \sin^2\left(\frac{\Omega_2 \Omega_3' t}{4\Omega_1}\right). \quad (32d)$$

Thus, the occupation probabilities  $|c_{-1}^{\uparrow}(t)|^2$ ,  $|c_{-1}^{\downarrow}(t)|^2$ ,  $|c_1^{\uparrow}(t)|^2$ , and  $|c_1^{\downarrow}(t)|^2$  show oscillatory behavior on different time scales. There is a fast frequency

$$2\Omega_2 = \frac{q^2 \hat{E}^2 \lambda^2}{(2\pi)^2 \hbar m c^2}, \quad (33)$$

an intermediate frequency

$$2\Omega_3' = \frac{q^2 \hat{E}^2 \lambda \sin \eta}{2\pi m^2 c^3}, \quad (34)$$

and a slow frequency

$$\frac{\Omega_2 \Omega_3'}{2\Omega_1} = \frac{q^4 \hat{E}^4 \lambda^5 \sin \eta}{(2\pi)^5 \hbar^2 m^2 c^5}. \quad (35)$$

The fast oscillation's amplitude is modulated by the intermediate-frequency oscillation, and the fast oscillation's amplitude and the intermediate oscillation's amplitude are modulated by the slow-frequency oscillation. The superposition of these three amplitude-modulated oscillations creates a nontrivial temporal behavior of the occupation probabilities (see also Fig. 2).

For  $\eta = 0$ , i. e.,  $\Omega_3' = 0$ , Eq. (32) simplifies to the known result for the Kapitza-Dirac effect with linearly polarized light [13].

For nonzero ellipticity, however, quantum transitions occur not only between states with different momenta but also between states with different spin orientations. As a consequence, the standing wave's ellipticity induces a beating behavior of the non-spin-resolved probabilities, i. e.,

$$|c_{-1}^{\uparrow}(t)|^2 + |c_{-1}^{\downarrow}(t)|^2 \approx \frac{1}{2}(1 + \cos(2\Omega_2 t) \cos(2\Omega_3' t)) = \frac{1}{2} \cos^2((\Omega_2 + \Omega_3')t) + \frac{1}{2} \cos^2((\Omega_2 - \Omega_3')t), \quad (36)$$

$$|c_1^{\uparrow}(t)|^2 + |c_1^{\downarrow}(t)|^2 \approx \frac{1}{2}(1 - \cos(2\Omega_2 t) \cos(2\Omega_3' t)) = \frac{1}{2} \sin^2((\Omega_2 + \Omega_3')t) + \frac{1}{2} \sin^2((\Omega_2 - \Omega_3')t). \quad (37)$$

With (29) the spin expectation value

$$\langle s(t) \rangle = \frac{\hbar}{2} (|c_{-1}^{\uparrow}(t)|^2 - |c_{-1}^{\downarrow}(t)|^2 + |c_1^{\uparrow}(t)|^2 - |c_1^{\downarrow}(t)|^2) \quad (38)$$

is given by

$$\langle s(t) \rangle = \frac{\hbar}{4} (\cos((\varepsilon_1 - \varepsilon_3)t) + \cos((\varepsilon_2 - \varepsilon_4)t)), \quad (39)$$

which may be simplified to

$$\langle s(t) \rangle \approx \frac{\hbar}{2} \cos(2\Omega_3' t) \cos\left(\frac{\Omega_2 \Omega_3'}{2\Omega_1} t\right) \quad (40)$$

by employing

$$\varepsilon_1 - \varepsilon_3 \approx 2\Omega_3' - \frac{\Omega_2 \Omega_3'}{2\Omega_1}, \quad (41a)$$

$$\varepsilon_2 - \varepsilon_4 \approx 2\Omega_3' + \frac{\Omega_2 \Omega_3'}{2\Omega_1}. \quad (41b)$$

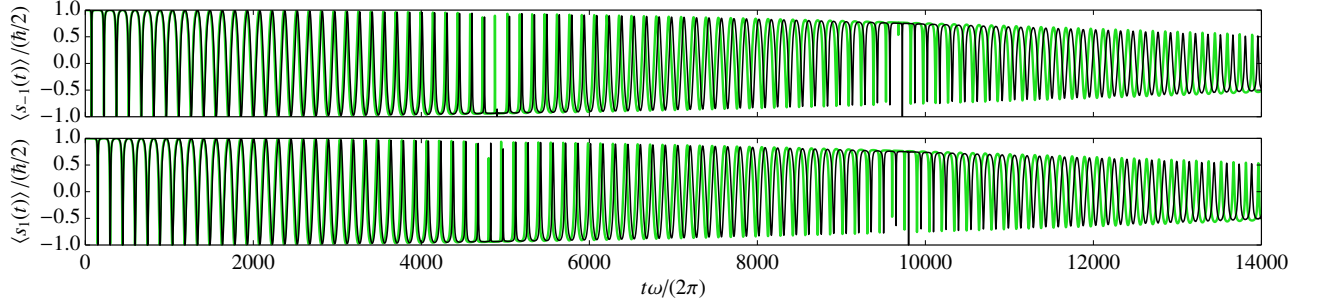


**FIG. 3:** (Color online) Time evolution of the spin of the two diffraction modes. Green (gray) lines show, from top to bottom, the analytical results (42) and (43) based on the relativistic Pauli equation (17). Black lines show the corresponding numerical results based on the Dirac equation (5). Parameters are as in Fig. 2.

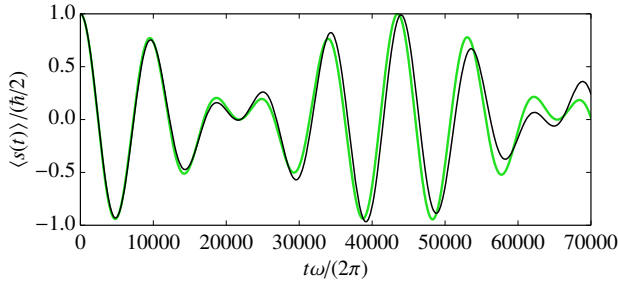


**FIG. 4:** (Color online) Time evolution of the electron's spin. Green (gray) line shows the analytical result (40) based on the relativistic Pauli equation (17). Black line shows the corresponding numerical data based on the Dirac equation (5). Parameters are as in Fig. 2.

Thus, in contrast to the Kapitza-Dirac effect with linearly polarized light, the electron's spin precesses in a standing wave of elliptical polarization. If the spin is conditioned to a specific mode, let us say  $n = -1$ , one finds

$$\begin{aligned} \langle s_{-1}(t) \rangle &= \frac{\hbar}{2} \frac{|c_{-1}^{\uparrow}(t)|^2 - |c_{-1}^{\downarrow}(t)|^2}{|c_{-1}^{\uparrow}(t)|^2 + |c_{-1}^{\downarrow}(t)|^2} \\ &\approx \frac{\hbar}{2} \frac{\cos\left(\frac{\Omega_2 \Omega_3'}{2\Omega_1} t\right) (\cos(2\Omega_2 t) + \cos(2\Omega_3' t))}{\cos(2\Omega_2 t) \cos(2\Omega_3' t) + 1}, \end{aligned} \quad (42)$$

and, similarly, for  $n = 1$

$$\begin{aligned} \langle s_1(t) \rangle &= \frac{\hbar}{2} \frac{|c_1^{\uparrow}(t)|^2 - |c_1^{\downarrow}(t)|^2}{|c_1^{\uparrow}(t)|^2 + |c_1^{\downarrow}(t)|^2} \\ &\approx \frac{\hbar}{2} \frac{\cos\left(\frac{\Omega_2 \Omega_3'}{2\Omega_1} t\right) (\cos(2\Omega_2 t) - \cos(2\Omega_3' t))}{\cos(2\Omega_2 t) \cos(2\Omega_3' t) - 1}. \end{aligned} \quad (43)$$

The analytical results, which have been obtained by deriving an approximate solution to the relativistic Pauli equation (17), shall be compared to numerical solutions of the time-dependent Dirac equation (5) with space- and time-dependent electromagnetic potentials. Figure 2 presents the probabilities to find the electron, which interacts with a standing light wave of the corotating setup, in one of the quantum states  $\psi_{-1}^{\uparrow}$ ,

$\psi_{-1}^{\downarrow}$ ,  $\psi_1^{\uparrow}$ , and  $\psi_1^{\downarrow}$  and compares this to the analytical predictions (32a) to (32d). Even for rather long interaction times the analytical results (32a) to (32d) match the fully relativistic dynamics as predicted by the Dirac equation. For the time evolution of the expectation value of the spin of the two diffraction modes,  $\langle s_{-1}(t) \rangle$  and  $\langle s_1(t) \rangle$ , as well as for the time evolution of the expectation value of the spin  $\langle s(t) \rangle$  we also find excellent agreement between the Dirac theory and (42), (43), and (40), respectively (see Figs. 3 and 4). The spin expectation values (40), (42), and (43) oscillate on different time scales. Because  $\Omega_2 > \Omega_3'$ , the shortest time scale of the total spin's oscillation, which is determined by the frequency  $2\Omega_3'$ , is longer than the time scale of the oscillation of (42) and (43), which is determined by  $2\Omega_2$ . Note that the electron's spin precesses faster in the Kapitza-Dirac effect compared to nonresonant scattering at the same field configuration, where the spin precesses with the frequency  $\Omega_2 \Omega_3' / (2\Omega_1)$  (see Refs. [29, 30] and the Appendix).

Although we employed in the presented numerical examples for the Kapitza-Dirac dynamics ultra strong laser parameters in the soft x-ray regime, the observed electron-spin dynamics is not a strong-field effect. Spin flips in the diffracted beam may be observed also for less intense laser fields, but the spin-precession frequency becomes small in this regime. In this case the electron must be trapped for many laser cycles in the laser field's focus to observe a full spin flip. The detectability of spin effects depends on the sensitivity of the spin measurement and for how long the electron interacts with the electromagnetic field. If one requires that the electron shall have reached full spin flip after  $\mathcal{N}$  laser periods and the laser parameters remain in the Bragg regime, then the required electric field strength is bounded from below and from above as

$$\sqrt{\frac{\omega^3 \hbar m}{2q^2 \mathcal{N}}} < \hat{E} \ll \frac{\omega^2 \hbar}{|q|c}. \quad (44)$$

Here the lower bound follows from  $\mathcal{N} > \omega / (4\Omega_2)$ , with  $2\Omega_2$  determining the shorter time scale of the spin dynamics of the diffracted electron beam. Note that the condition (44) is much less restrictive than the corresponding relation for the nonresonant scattering as presented in Ref. [30].

According to Eq. (40) the electron's spin oscillates with the frequency  $2\Omega_3 \sin \eta$ , which is modulated by an oscillation with the frequency  $\Omega_2 \Omega_3 \sin \eta / (2\Omega_1)$ . This allows us to test

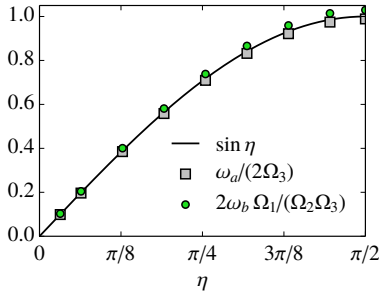


**FIG. 5:** (Color online) Spin-oscillation frequencies for different degrees of ellipticity  $\eta$  as obtained by a numerical fit procedure to data of numerical solutions of the Dirac equation compared to the predictions by the relativistic Pauli equation (17). Parameters are as in Fig. 2.

the effect of the light's ellipticity  $\eta$  on the Kapitza-Dirac effect. For this purpose the numerical data for the spin expectation value as a function of the interaction time were fitted to  $\hbar \cos(\omega_a t) \cos(\omega_b t)/2$  with the fit parameters  $\omega_a$  and  $\omega_b$ . In Fig. 5 the numerical values of these fit parameters are compared to  $2\Omega_3$  and  $\Omega_2\Omega_3/(2\Omega_1)$ . The numerical data show a clear  $\sin \eta$  dependency, as predicted by our analytical considerations.

## 4.2. Antiroating fields

For the setup with antirotating fields, which is described by (20), the ansatz (21) gives the following set of equations in momentum space:

$$i\hbar \dot{c}_n(t) = \frac{n^2 k^2 \hbar^2}{2m} c_n(t) + \frac{q^2 \hat{E}^2 \cos \eta}{2k^2 mc^2} (c_{n-2}(t) + 2c_n(t) + c_{n+2}(t)). \quad (45)$$

Similar to the corotating case, only odd and even modes couple to each other, and furthermore, modes corresponding to different spin orientations are decoupled. Truncating the system (45) to

$$i \begin{pmatrix} \dot{c}_{-1}^\uparrow(t) \\ \dot{c}_{-1}^\downarrow(t) \\ \dot{c}_1^\uparrow(t) \\ \dot{c}_1^\downarrow(t) \end{pmatrix} = \begin{pmatrix} \Omega_1 & 0 & \Omega_2' & 0 \\ 0 & \Omega_1 & 0 & \Omega_2' \\ \Omega_2' & 0 & \Omega_1 & 0 \\ 0 & \Omega_2' & 0 & \Omega_1 \end{pmatrix} \begin{pmatrix} c_{-1}^\uparrow(t) \\ c_{-1}^\downarrow(t) \\ c_1^\uparrow(t) \\ c_1^\downarrow(t) \end{pmatrix} \quad (46)$$

with  $\Omega_2' = \Omega_2 \cos \eta$  yields, for the initial condition  $c_{-1}^\uparrow(0) = 1$  and  $c_n^\gamma(0) = 0$  otherwise, the exact solution

$$c_{-1}^\uparrow(t) = \cos(\Omega_1 t) \cos(\Omega_2' t) - i \sin(\Omega_1 t) \cos(\Omega_2' t), \quad (47a)$$

$$c_{-1}^\downarrow(t) = 0, \quad (47b)$$

$$c_1^\uparrow(t) = -\sin(\Omega_1 t) \sin(\Omega_2' t) - i \cos(\Omega_1 t) \sin(\Omega_2' t), \quad (47c)$$

$$c_1^\downarrow(t) = 0. \quad (47d)$$

The probabilities  $|c_{-1}^\uparrow(t)|^2$  and  $|c_1^\uparrow(t)|^2$  follow as

$$|c_{-1}^\uparrow(t)|^2 = \cos^2(\Omega_2' t), \quad (48a)$$

$$|c_1^\uparrow(t)|^2 = \sin^2(\Omega_2' t). \quad (48b)$$

Thus, the probabilities oscillate with the Rabi frequency

$$2\Omega_2' = \frac{q^2 \hat{E}^2 \lambda^2 \cos \eta}{(2\pi)^2 \hbar mc^2}, \quad (49)$$

which is known as the Rabi frequency of the Kapitza-Dirac effect with linearly polarized light, modified by the factor  $\cos \eta$ .

As a consequence of (49), a nonvanishing ellipticity decreases the Rabi frequency. In the case of circular polarization it even becomes zero; that is, Kapitza-Dirac scattering is completely suppressed. To test this analytical prediction we fitted the probability to find the electron in the quantum state  $\psi_{-1}^\uparrow$  as obtained from the numerical solution of the Dirac equation to the function  $\cos^2(\omega_a t)$  with the fit parameter  $\omega_a$ . The numerical values for  $\omega_a$  are compared to  $\Omega_2'$  for different values of  $\eta$  in Fig. 6, which shows a clear  $\cos \eta$  dependency, as predicted by our analytical considerations.

As demonstrated above, the dynamics of the electron in the antirotating setup can be modeled by a time-independent scalar potential, which may be understood by classical arguments. Consider a charged particle in the antirotating fields. The classical motion of the particle is determined by the Lorentz force

$$\ddot{\mathbf{r}} = \frac{q}{m} (\mathbf{E}^{\zeta\zeta}(x, t) + \dot{\mathbf{r}} \times \mathbf{B}^{\zeta\zeta}(x, t)). \quad (50)$$

The velocity  $\dot{\mathbf{r}}$  may be divided into two parts,  $\dot{\mathbf{r}} = \dot{\mathbf{r}}_{\parallel} + \dot{\mathbf{r}}_{\perp}$ , that are parallel to the  $x$  axis and perpendicular to the  $x$  axis, respectively. The change of the latter is primarily determined by the electrical field

$$\ddot{\mathbf{r}}_{\perp} = \frac{q}{m} \mathbf{E}^{\zeta\zeta}(x, t). \quad (51)$$

Integrating this equation of motion yields the perpendicular velocity

$$\dot{\mathbf{r}}_{\perp} = \frac{2q\hat{E}}{m\omega} \sin(\omega t) \begin{pmatrix} 0 \\ \cos(kx) \\ \cos(kx + \eta) \end{pmatrix} + \dot{\mathbf{r}}_{\perp}(0). \quad (52)$$

The motion along the  $x$  axis is solely determined by the magnetic field, i. e.,

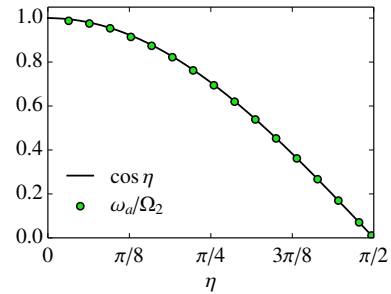


**FIG. 6:** (Color online) Rabi oscillation frequencies for different degrees of ellipticity  $\eta$  for the antirotating setup as obtained by a numerical fit procedure to data of numerical solutions of the Dirac equation compared to the predictions by the relativistic Pauli equation (17). Parameters are as in Fig. 2.

$$\begin{aligned}\ddot{\mathbf{r}}_{\parallel} &= \frac{q}{m} \dot{\mathbf{r}}_{\perp} \times \mathbf{B}^{\text{TL}}(x, t) \\ &= \frac{4q^2 \hat{E}^2 \sin^2(\omega t)}{m^2 c \omega} \begin{pmatrix} 0 \\ \cos(kx) \\ \cos(kx + \eta) \end{pmatrix} \times \begin{pmatrix} 0 \\ -\sin(kx + \eta) \\ \sin(kx) \end{pmatrix} \\ &\quad + \frac{q}{m} \dot{\mathbf{r}}_{\perp}(0) \times \mathbf{B}^{\text{TL}}(x, t) \mathbf{e}_x. \quad (53)\end{aligned}$$

Because the velocity  $\dot{\mathbf{r}}_{\perp}$  is in phase with the magnetic field and both are proportional to  $\sin(\omega t)$ , the acceleration parallel to the  $x$  axis does not average out over a laser cycle. Only the effect of the last term in Eq. (53) cancels for sufficiently long interaction times. The value of the nonvanishing contribution depends crucially on the spatial phase relation between the electric field, which is  $\sim (0, \cos(kx), \cos(kx + \eta))^{\text{T}}$ , and the magnetic field, which is  $\sim (0, -\sin(kx + \eta), \sin(kx))^{\text{T}}$ . Thus, the time-averaged acceleration parallel to the  $x$  axis

$$\ddot{\mathbf{r}}_{\parallel} \approx \frac{2q^2 \hat{E}^2}{m^2 c \omega} \cos \eta \sin(2kx + \eta) \mathbf{e}_x \quad (54)$$

and the corresponding potential

$$V_{\text{pond}} = \frac{2q^2 \hat{E}^2}{m \omega^2} \cos \eta \cos^2(kx + \eta/2) \quad (55)$$

are proportional to  $\cos \eta$ , which causes the  $\cos \eta$  dependency of the Rabi frequency (49).

## 5. Conclusions

We studied the two-photon Kapitza-Dirac effect in the Bragg regime for setups with counterpropagating elliptically polarized electromagnetic waves whose electric-field components may have the same or an opposite sense of rotation. The time-dependent fully relativistic Dirac equation was solved numerically to simulate the electron's dynamics. To allow for an analytical description of the scattering process the explicitly time-dependent Dirac-equation Hamiltonian was reduced to an effective time-independent eight-level Hamiltonian or four-level Hamiltonian by approximating the Dirac equation by the Pauli equation plus the leading relativistic corrections and employing suitable ponderomotive potentials. In the parameter range of the Bragg regime, the fully relativistic Dirac equation and the effective time-independent Hamiltonian give qualitatively the same results, which also agree quantitatively very well for not too long interaction times.

The light waves' ellipticity does not change the Bragg condition compared to the case of linear polarization. It induces, however, spin dynamics in the case of corotating counterpropagating waves. The spin's expectation value of the quantum-mechanical superposition of the scattered and nonscattered states precesses with a period which is larger than the Rabi period of the Kapitza-Dirac scattering. The projections of the electron's quantum state onto the scattering and nonscattering channels, however, show spin precession on the time scale of the Rabi period of Kapitza-Dirac scattering. The precession of the electron's spin is induced equally by the Zeeman

interaction and the electron-spin's coupling to the photonic spin density of the standing light wave. This effect may be observable by employing upcoming laser sources for circularly polarized light [45] with wavelength and intensity parameters as utilized by Freimund et al. [9], provided that the electron interacts long enough with the electromagnetic field to rotate the spin. Compared to nonresonant scattering [29, 30], where spin precession is also induced by the elliptically polarized light wave, the spin-precession frequency is substantially faster for the Kapitza-Dirac effect. Thus, shorter interaction times are required to observe spin-precession experimentally.

Antirotating counterpropagating waves yield a standing wave with linear polarization, i. e., vanishing photonic spin density; thus, no spin effects can be observed for this kind of setup. However, the phase between the electric and the magnetic-field components of the standing wave depends on the ellipticity of the counterpropagating laser fields, and in this way the Rabi period of Kapitza-Dirac scattering depends on the ellipticity. This Rabi period diverges in the limit of circular polarization; that is, the Kapitza-Dirac effect cannot be observed in the antirotating setup for circular polarization.

## A. Nonresonant scattering

Recently, it was shown [30] that the coupling of the spin angular momentum of light beams with elliptical polarization to the spin degree of freedom of free electrons can lead to spin precession. The spin-precession frequency was derived by a tedious calculation based on time-dependent perturbation theory. The setup that was considered in Refs. [29, 30] is identical to the corotating field configuration, which was analyzed in Sec. 4.1, except that the electron is initially at rest; that is, it does not fulfill the Bragg condition of the Kapitza-Dirac effect. In the following we will show that the spin-precession frequency of [30] can be derived easily by employing the time-independent Hamiltonian in Eq. (17).

Equation (23) yields, for the even modes, the truncated system

$$i \begin{pmatrix} \dot{c}_{-2}^{\uparrow}(t) \\ \dot{c}_{-2}^{\downarrow}(t) \\ \dot{c}_0^{\uparrow}(t) \\ \dot{c}_0^{\downarrow}(t) \\ \dot{c}_2^{\uparrow}(t) \\ \dot{c}_2^{\downarrow}(t) \end{pmatrix} = \begin{pmatrix} 4\Omega_1 & 0 & \Omega_2 & \Omega_3' & 0 & 0 \\ 0 & 4\Omega_1 & \Omega_3' & \Omega_2 & 0 & 0 \\ \Omega_2 & \Omega_3' & 0 & 0 & \Omega_2 & \Omega_3' \\ \Omega_3' & \Omega_2 & 0 & 0 & \Omega_3' & \Omega_2 \\ 0 & 0 & \Omega_2 & \Omega_3' & 4\Omega_1 & 0 \\ 0 & 0 & \Omega_3' & \Omega_2 & 0 & 4\Omega_1 \end{pmatrix} \begin{pmatrix} c_{-2}^{\uparrow}(t) \\ c_{-2}^{\downarrow}(t) \\ c_0^{\uparrow}(t) \\ c_0^{\downarrow}(t) \\ c_2^{\uparrow}(t) \\ c_2^{\downarrow}(t) \end{pmatrix}. \quad (\text{A.1})$$

As for the Kapitza-Dirac effect the eigenvalues and the eigenvectors of the coefficient matrix in Eq. (A.1) can be calculated exactly, which gives the exact eigenvalues

$$\varepsilon_{1,2} = 2\Omega_1 - \sqrt{4\Omega_1^2 + 2(\Omega_2 \pm \Omega_3')^2}, \quad (\text{A.2a})$$

$$\varepsilon_{3,4} = 4\Omega_1, \quad (\text{A.2b})$$

$$\varepsilon_{5,6} = 2\Omega_1 + \sqrt{4\Omega_1^2 + 2(\Omega_2 \pm \Omega_3')^2}. \quad (\text{A.2c})$$

However, we replace the exact eigenvectors by the approximate eigenvectors

$$(v_1 \ v_2 \ v_3 \ v_4 \ v_5 \ v_6) = \begin{pmatrix} 0 & 0 & \frac{1}{\sqrt{2}} & 0 & \frac{1}{2} & \frac{1}{2} \\ 0 & 0 & 0 & \frac{1}{\sqrt{2}} & \frac{1}{2} & -\frac{1}{2} \\ \frac{1}{\sqrt{2}} & \frac{1}{\sqrt{2}} & 0 & 0 & 0 & 0 \\ \frac{1}{\sqrt{2}} & -\frac{1}{\sqrt{2}} & 0 & 0 & 0 & 0 \\ 0 & 0 & -\frac{1}{\sqrt{2}} & 0 & \frac{1}{2} & \frac{1}{2} \\ 0 & 0 & 0 & -\frac{1}{\sqrt{2}} & \frac{1}{2} & -\frac{1}{2} \end{pmatrix}. \quad (\text{A.3})$$

Specifying  $c_0^\uparrow(0) = 1$  and  $c_n^\gamma(0) = 0$  otherwise as the initial condition and approximating the eigenvectors of the coefficient matrix in Eq. (A.1) by (A.3) yields the time-dependent solution to (A.1),

$$c_2^\uparrow(t) = 0, \quad (\text{A.4a})$$

$$c_2^\downarrow(t) = 0, \quad (\text{A.4b})$$

$$c_0^\uparrow(t) = \frac{1}{2} (e^{-i\varepsilon_1 t} + e^{-i\varepsilon_2 t}), \quad (\text{A.4c})$$

$$c_0^\downarrow(t) = \frac{1}{2} (e^{-i\varepsilon_1 t} - e^{-i\varepsilon_2 t}), \quad (\text{A.4d})$$

$$c_2^\uparrow(t) = 0, \quad (\text{A.4e})$$

$$c_2^\downarrow(t) = 0. \quad (\text{A.4f})$$

The evolution of the probabilities  $|c_0^\uparrow(t)|^2$  and  $|c_0^\downarrow(t)|^2$  is with (A.4)

$$|c_0^\uparrow(t)|^2 = \cos^2\left(\frac{\varepsilon_2 - \varepsilon_1}{2} t\right), \quad (\text{A.5a})$$

$$|c_0^\downarrow(t)|^2 = \sin^2\left(\frac{\varepsilon_2 - \varepsilon_1}{2} t\right). \quad (\text{A.5b})$$

Considering again the regime (24), the approximation

$$\varepsilon_2 - \varepsilon_1 \approx \frac{2\Omega_2\Omega_3'}{\Omega_1} \quad (\text{A.6})$$

holds. Thus,

$$|c_0^\uparrow(t)|^2 \approx \cos^2\left(\frac{q^4 \hat{E}^4 \lambda^5 \sin \eta t}{(2\pi)^5 \hbar^2 m^2 c^5 2}\right), \quad (\text{A.7a})$$

$$|c_0^\downarrow(t)|^2 \approx \sin^2\left(\frac{q^4 \hat{E}^4 \lambda^5 \sin \eta t}{(2\pi)^5 \hbar^2 m^2 c^5 2}\right), \quad (\text{A.7b})$$

which represents exactly the Rabi oscillation of the electron spin as predicted in Refs. [29, 30].

- 
- [1] P. L. Kapitza and P. A. M. Dirac, *Math. Proc. Cambridge Philos. Soc.* **29**, 297 (1933).
- [2] H. Batelaan, *Contemp. Phys.* **41**, 369 (2000).
- [3] C. S. Adams, M. Sigel, and J. Mlynek, *Phys. Rep.* **240**, 143 (1994).
- [4] M. Freyberger, A. M. Herkommer, D. Krähmer, E. Mayr, and W. P. Schleich, *Adv. At., Mol., Opt. Phys.* **41**, 143 (1999).
- [5] P. L. Gould, G. A. Ruff, and D. E. Pritchard, *Phys. Rev. Lett.* **56**, 827 (1986).
- [6] P. J. Martin, B. G. Oldaker, A. H. Miklich, and D. E. Pritchard, *Phys. Rev. Lett.* **60**, 515 (1988).
- [7] S. Eilzer, H. Zimmermann, and U. Eichmann, *Phys. Rev. Lett.* **112**, 113001 (2014).
- [8] P. H. Bucksbaum, D. W. Schumacher, and M. Bashkansky, *Phys. Rev. Lett.* **61**, 1182 (1988).
- [9] D. L. Freimund, K. Aflatooni, and H. Batelaan, *Nature (London)* **413**, 142 (2001).
- [10] D. L. Freimund and H. Batelaan, *Phys. Rev. Lett.* **89**, 283602 (2002).
- [11] M. A. Efremov and M. V. Fedorov, *J. Phys. B: At., Mol. Opt. Phys.* **33**, 4535 (2000).
- [12] X. Li, J. Zhang, Z. Xu, P. Fu, D.-S. Guo, and R. R. Freeman, *Phys. Rev. Lett.* **92**, 233603 (2004).
- [13] H. Batelaan, *Rev. Mod. Phys.* **79**, 929 (2007).
- [14] P. Sancho, *Phys. Rev. A* **82**, 033814 (2010).
- [15] P. Sancho, *J. Phys. B: At., Mol. Opt. Phys.* **44**, 145002 (2011).
- [16] M. M. Dellweg and C. Müller, *Phys. Rev. A* **91**, 062102 (2015).
- [17] S. McGregor, W. C.-W. Huang, B. A. Shadwick, and H. Batelaan, *Phys. Rev. A* **92**, 023834 (2015).
- [18] A. G. Hayrapetyan, K. K. Grigoryan, J. B. Götze, and R. G. Petrosyan, *New J. Phys.* **17**, 082002 (2015).
- [19] D. L. Freimund and H. Batelaan, *Laser Phys.* **13**, 892 (2003).
- [20] L. Rosenberg, *Phys. Rev. A* **70**, 023401 (2004).
- [21] S. Ahrens, H. Bauke, C. H. Keitel, and C. Müller, *Phys. Rev. Lett.* **109**, 043601 (2012).
- [22] S. Ahrens, H. Bauke, C. H. Keitel, and C. Müller, *Phys. Rev. A* **88**, 012115 (2013).
- [23] G. Mourou, N. Fisch, V. Malkin, Z. Toroker, E. Khazanov, A. Sergeev, T. Tajima, and B. Le Garrec, *Opt. Commun.* **285**, 720 (2012).
- [24] S. X. Hu and C. H. Keitel, *Phys. Rev. Lett.* **83**, 4709 (1999).
- [25] M. W. Walser, D. J. Urbach, K. Z. Hatsagortsyan, S. X. Hu, and C. H. Keitel, *Phys. Rev. A* **65**, 043410 (2002).
- [26] F. H. M. Faisal and S. Bhattacharyya, *Phys. Rev. Lett.* **93**, 053002 (2004).
- [27] G. Brodin, M. Marklund, J. Zamanian, and M. Stefan, *Plasma Phys. Controlled Fusion* **53**, 074013 (2011).
- [28] O. D. Skoromnik, I. D. Feranchuk, and C. H. Keitel, *Phys. Rev. A* **87**, 052107 (2013).
- [29] H. Bauke, S. Ahrens, C. H. Keitel, and R. Grobe, *New J. Phys.* **16**, 103028 (2014).
- [30] H. Bauke, S. Ahrens, and R. Grobe, *Phys. Rev. A* **90**, 052101 (2014).
- [31] A. Wöllert, H. Bauke, and C. H. Keitel, *Phys. Rev. D* **91**, 125026 (2015).
- [32] T.-O. Müller and C. Müller, *Phys. Rev. A* **86**, 022109 (2012).
- [33] I. Barth and O. Smirnova, *J. Phys. B: At., Mol. Opt. Phys.* **47**, 204020 (2014).
- [34] E. Yakoboylu, M. Klaiber, and K. Z. Hatsagortsyan, *Phys. Rev. A* **91**, 063407 (2015).
- [35] F. Gross, *Relativistic Quantum Mechanics and Field Theory* (Wiley-VCH, Weinheim, 2004).
- [36] B. Thaller, *Advanced Visual Quantum Mechanics* (Springer, Heidelberg, 2005).
- [37] J. W. Braun, Q. Su, and R. Grobe, *Phys. Rev. A* **59**, 604 (1999).
- [38] H. Bauke and C. H. Keitel, *Comput. Phys. Commun.* **182**, 2454 (2011).
- [39] L. L. Foldy and S. A. Wouthuysen, *Phys. Rev.* **78**, 29 (1950).
- [40] J. Fröhlich and U. M. Studer, *Rev. Mod. Phys.* **65**, 733 (1993).
- [41] W. Magnus, *Commun. Pure Appl. Math.* **7**, 649 (1954).
- [42] S. Blanes, F. Casas, J. Oteo, and J. Ros, *Phys. Rep.* **470**, 151 (2009).

- [43] A. L. Pokrovsky and A. E. Kaplan, *Phys. Rev. A* **72**, 043401 (2005).
- [44] P. W. Smorenburg, J. H. M. Kanters, A. Lassise, G. J. H. Brussaard, L. P. J. Kamp, and O. J. Luiten, *Phys. Rev. A* **83**, 063810 (2011).
- [45] A. Depresseux, E. Oliva, J. Gautier, F. Tissandier, G. Lambert, B. Vodungbo, J.-P. Goddet, A. Tafzi, J. Nejd, M. Kozlova, G. Maynard, H. T. Kim, K. T. Phuoc, A. Rousse, P. Zeitoun, and S. Sebban, *Phys. Rev. Lett.* **115**, 083901 (2015).